PCCP

ROYAL SOCIETY OF CHEMISTRY

PAPER

View Article Online
View Journal | View Issue

Cite this: *Phys. Chem. Chem. Phys.*, 2025, **27**, 8320

Tautomerism of a backbone protonated peptide revealed by soft X-ray action spectroscopy†

Juliette Leroux, [abc] Carlos Ortiz-Mahecha, [d] Kaja Schubert, [b] Florian Trinter, [e] Isaak Unger, [f] Lucas Schwob [b] and Sadia Bari *[bg]

Received 7th February 2025,
Accepted 27th March 2025

DOI: 10.1039/d5cp00506j

rsc.li/pccp

The structure and reactivity of peptides can be influenced by their protonation state. Notably, protonation of the backbone can induce structural changes, such as tautomerism, shifting from the stable keto form to the enol form. This phenomenon, particularly in the backbone protonated peptide acetyl-pentaglycine, was examined using a combination of soft X-ray action spectroscopy at the nitrogen K-edge and theoretical calculations based on density functional theory (DFT). We identified a resonance at 400 eV that can be clearly attributed to π*(C═N) transitions, linked exclusively to the enol form, as no keto form structures could replicate this resonance. These findings enhanced our understanding of the effect of protonation on the structure of peptides and could be employed for future dynamic studies.

1 Introduction

In biological media, the charge state of, *e.g.*, peptides plays a crucial role in determining their structure and reactivity. In particular, protonation and deprotonation can alter the hydrogen bonding network among the amino acids, thereby affecting the peptide's folding and stability.[1] Localizing the (de-)protonation sites and evaluating their impact on the structure of peptides is essential for advancing our knowledge of biological processes and the relationship between structure and function.

For protonated peptides, the protonation usually occurs at the nitrogen site of the N-terminus or at basic sites.[2–5] However, when a peptide with a capped N-terminus does not contain a basic side chain, the proton will likely bind on one of the amide oxygen atoms.[6] It has been shown that for a simple tripeptide, triglycine, protonation on the backbone and protonation on the nitrogen atom (N-terminus) can coexist.[7–9] Being part of the biological medium, peptides interact with an aqueous solvent, which can influence the structure and act as a catalyst for proton transfer that could cause tautomerism of the peptide structure from the most stable keto form to its enol form.[10] In peptides, proton transfer can favor the enol formation through proton wiring keto–enol tautomerism.[11,12]

Keto–enol tautomerism of a peptide bond, [–CONH–], is defined by a proton migration from a carbon or nitrogen atom to an oxygen atom, forming a C═N double bond and a C–OH single bond, written as a [–C(OH)N–] form.[13–15] This process has been extensively studied on β-diketone, acetylacetone, phenyl-containing molecules, and peptides in the liquid and gas phases by infrared (IR) spectroscopy, X-ray diffraction, photoemission spectroscopy, and density functional theory (DFT) calculations.[7,12,16–22] In most cases, the keto tautomers are more stable than their enol form by around 0.85 eV, with calculated energy barriers indicating slow interconversions,[12,18] and the enolization of the molecule is induced by the solvent or by activation such as UV photoabsorption.[11,12,16,20,23]

The presence of enol bonds can be characterized using spectroscopic methods. Enolization results in the appearance of a new absorption band in the IR spectrum.[17,23] Using X-ray photoemission spectroscopy, it is possible to quantify the keto–enol tautomerism of a tripeptide (IGF) by measuring the ratio of two experimental resonances at the nitrogen (400.3 eV and 401.7 eV) and oxygen (531.6 eV and 533.2 eV) K-edges.[23] Moreover, soft X-ray absorption is element-specific, and spectroscopy in the energy region of the carbon, nitrogen, and oxygen K-edges has been used to study the electronic structure of biomolecular systems.[24–28] Near-edge X-ray absorption mass spectrometry (NEXAMS) has been developed for studying larger protonated biomolecules in the gas phase.[9,29–32] In particular, it has been demonstrated that NEXAMS is sensitive to the protonation site of oligonucleotides and peptides.[9,31] It has

[a] *CIMAP, CEA/CNRS/ENSICAEN/Université de Caen Normandie, 14050 Caen, France*
[b] *Deutsches Elektronen-Synchrotron DESY, 22603 Hamburg, Germany. E-mail: sadia.bari@desy.de*
[c] *Department of Physics, University of Hamburg, 22607 Hamburg, Germany*
[d] *Institute for Interface Physics and Engineering, Technische Universität Hamburg, 21073 Hamburg, Germany*
[e] *Molecular Physics, Fritz-Haber-Institut der Max-Planck-Gesellschaft, 14195 Berlin, Germany*
[f] *Department of Physics and Astronomy, Uppsala University, 75120 Uppsala, Sweden*
[g] *Zernike Institute for Advanced Materials, University of Groningen, 9747 AG Groningen, The Netherlands*

† Electronic supplementary information (ESI) available. See DOI: https://doi.org/10.1039/d5cp00506j

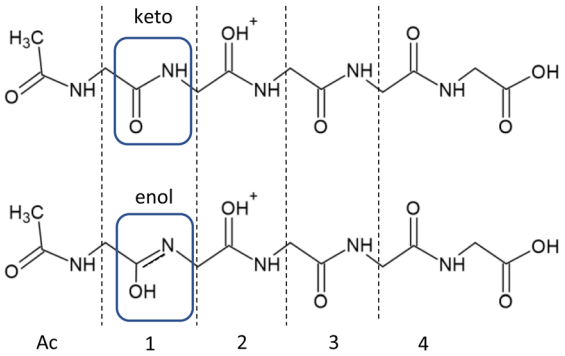

Fig. 1 Top: Chemical structure of acetyl-G_5 protonated on the second peptide bond oxygen atom (named $\mathbf{P_2}$ in the following). Bottom: Chemical structure of acetyl-G_5 protonated on the second peptide bond oxygen atom with an enol form on the first peptide bond (named $\mathbf{P_2E_1}$ in the following). The four peptide bonds and the acetyl group that can be protonated or subject to enolization are marked 1, 2, 3, or 4, and Ac.

been shown for peptide-like molecules that soft X-ray absorption techniques can be used to differentiate, at the N K-edge, the electronic resonances of $\pi^*_{C=N}$ and $\pi^*_{C=O}$ excitations.[28] From an earlier study, it has been suggested for a pentapeptide, methionine enkephalin, that the resonance of an enol form of a peptide bond in a peptide should be observed at around 399.2 eV.[30]

The aim of this work is twofold: (1) record unambiguously the electronic signature of a backbone protonated peptide, therefore completing our previous work on protonated peptides,[9] and (2) assess the change in electronic structure induced by keto–enol tautomerism of a peptide bond as may be induced by backbone protonation. To these ends, we performed NEXAMS measurements at the nitrogen K-edge of protonated acetyl-pentaglycine (denoted Ac-G_5 in the following), whose structure is shown in Fig. 1. Ac-G_5 has no basic side chain and a capped N-terminus; thus, we expect protonation on an amide oxygen atom.[6] Moreover, it is expected that the proton is not fixed on a specific oxygen atom but is mobile through the peptide backbone;[6,7] it could induce keto–enol tautomerism as depicted in Fig. 1. This paper is divided as follows: first, the experimental and theoretical methods are explained. Then, the experimental NEXAMS spectrum at the nitrogen K-edge is described and compared with its uncapped relative structure, pentaglycine (G_5), which we have previously investigated.[9] In the last section, the potential structural candidates are discussed in light of the comparison between our experimental and simulation results.

2 Methods

2.1 Experimental methods

Ac-G_5 was purchased from ProteoGenix (Schiltigheim, France) at >95% purity and used without further purification. The sample solution was prepared at 30 μM concentration in 1 : 1 water/methanol with 1% of formic acid to ensure protonation.

The experimental spectrum was obtained during a measurement campaign by coupling our home-built tandem mass spectrometer to the P04 soft X-ray beamline at the PETRA III synchrotron (DESY, Hamburg, Germany).[33] Briefly, the setup relies on a high-fluence electrospray ionization (ESI) source to introduce the ions into the gas phase. The electrosprayed ions are transported by a heated capillary into the first pumping stage, which hosts a radio frequency (RF) ion funnel to guide and focus the ions. The ions continue through an RF octupole ion guide to a quadrupole mass filter (QMS), where the ions of interest are selected according to their mass-to-charge (m/z) ratio. Then, a second RF octupole and a set of Einzel lenses guide and focus the ions into an RF 3D ion trap, where they are accumulated before irradiation with photons. To allow for efficient trapping of the ions, their kinetic energy is cooled down by collisions with a helium buffer gas, with a pressure in the trap of around 5×10^{-5} mbar. After irradiation with X-ray photons for 2 seconds, all cationic products are extracted from the trap and analyzed in a reflectron time-of-flight (Re-TOF) mass spectrometer ($m/\Delta m$ = 1800). A schematic of the experimental setup is shown in Fig. 2.

At the N K-edge, the photon-energy bandwidth was set to 250 meV. The photon-energy scans were performed by steps of 200 meV across the N K-edge (397–411 eV). A photodiode placed downstream of the ion trap was used to record the photon flux. The NEXAMS spectra obtained were normalized to the photon flux and the precursor ion intensity to correct for ESI source fluctuations. To account for all sources of background ions, the data acquisition was divided into repeated cycles of three mass scans. First, a mass spectrum of the ESI only was recorded to measure the precursor ion intensity and fragments originating from energetic collisions with the buffer gas and to evaluate the precursor ion intensity for normalization. Second, the mass spectrum resulting from irradiation of the trapped molecules was recorded. For the third spectrum, the target ion beam is blocked by applying a high voltage (typically 50 V) on the electrode at the exit of the octupole, and the mass spectrum resulting from the irradiation of the residual gas was recorded. The mass spectrum resulting from the ESI and the one resulting from the irradiation of the residual gas were subtracted from the mass spectrum resulting from the irradiation of the trapped molecules. A series of hundred cycles was accumulated to average over long-term fluctuations in the source and to obtain the final mass spectrum, shown in Fig. S1 (ESI†).

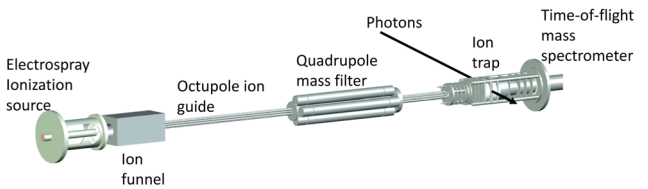

Fig. 2 Schematic of our experimental setup used to record the NEXAMS spectrum of Ac-G_5.

2.2 Theoretical calculations

The X-ray absorption spectra of protonated acetyl-pentaglycine candidates were calculated, assigning the resonances in the absorption spectrum at the nitrogen K-edge. All calculations were performed using the (time-dependent) density functional theory (DFT) method, employing the TZVP Ahlrichs basis set[34] in combination with the B3LYP exchange–correlation functional[35] using the ORCA electronic-structure package.[36] Relativistic effects were considered using the zeroth order regular approximation (ZORA).[37] Based on the experimental findings, we propose that Ac-G_5 may undergo protonation at the oxygen atoms of the peptide bonds and can also be present in enol forms (see next section). Thus, we computed all possible protonation sites and enol forms from an initial folded structure of Ac-G_5. This analysis identifies five possible protonation sites (on all four amide oxygen atoms from the peptide bonds and on the oxygen atom of the acetyl group) with four enol forms for each protonation site. Structures having multiple peptide bonds in enol forms were omitted, as they were less stable than those with single enol tautomers, which were already around 0.5 eV higher in energy than the keto interconvert forms. All structures were further optimized using DFT, and their calculated absorption spectra at the N K-edge were calculated using TDDFT. The final X-ray absorption spectra were broadened using a Gaussian profile with a full width at half maximum (FWHM) of 0.6 eV to account for the experimental photon-energy resolution, the core–hole lifetime, and the electronic broadening of the transitions.[38,39] An energy shift of 12.5 eV was applied to the calculated absorption spectra to account for the difference between the experimental and the simulated results. This shift was determined by matching the energy of the experimental resonance at 401.7 eV (N 1s → π*(CONH) as explained later) with its calculated representative.

3 Results and discussion

3.1 Absorption spectra at the nitrogen K-edge

G_5 has been described in detail in our previous study on peptide protonation.[9] It has an unambiguous protonation site located on the N-terminus, which makes G_5 a good reference model for this study as we expect backbone protonation to have a different signature at the N K-edge.

The NEXAMS spectrum of G_5, shown in Fig. 3, shows a first resonance at 401.6 eV stemming from the N 1s → π*(CONH) transitions within peptide bonds. A second resonance is observed at 402.6 eV from N_i 1s → π*(CON_jH) where N_i and N_j are different nitrogen atoms in neighboring peptide bonds. A broad feature located around 406 eV is due to several transitions to σ* orbitals, including N 1s → σ*(NH_3^+) from the protonation site, here located on the N-terminus.[9,30,40] Therefore, the signature of the protonation site of G_5 is the broad and intense feature at around 406 eV.

In contrast to G_5, Ac-G_5, shown in Fig. 3, exhibits a remarkably different spectrum. Unlike G_5, the spectrum of Ac-G_5 includes two additional features before the resonance at

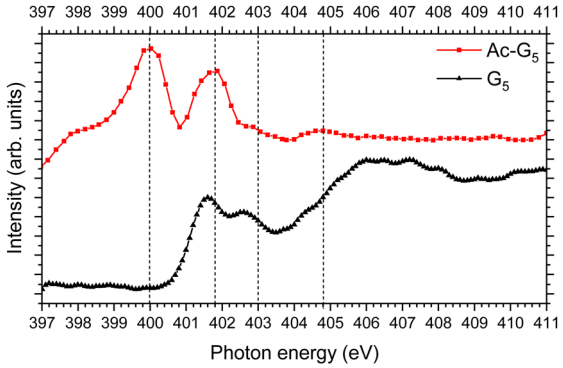

Fig. 3 Experimental absorption spectra of Ac-G_5 (red) and G_5 (black) at the nitrogen K-edge. Note that G_5 has been recorded at 210 meV bandwidth and with 100 meV energy steps.[9] Both spectra have been normalized on the intensity of the π*(CONH) resonance. An additional offset in the *y* axis has been applied to the Ac-G_5 spectrum for comparison purposes. Four vertical dashed lines, at 400 eV, 401.7 eV, 403 eV, and 404.8 eV, mark the main resonant excitation bands of Ac-G_5.

401.6 eV: a low-intensity feature at 398 eV and the most intense resonance at 400 eV. It is followed by a strong band at 401.7 eV and two weaker bands centered at 403 eV and 404.8 eV. As in the case of G_5, we can attribute the resonance at 401.7 eV to N 1s → π*(CONH) transitions within peptide bonds. The N_i 1s → π*(CON_jH) resonance present at 402.6 eV in the case of G_5 is not observed for Ac-G_5, although we cannot exclude that these resonances are part of the band at 403 eV in Ac-G_5, thus blueshifted by 0.4 eV compared to G_5. This band could also be the result of a transition from an N 1s → σ*(CH) excitation from the backbone, as already observed for protonated triglycine.[9] The resonance at 404.8 eV could be attributed to N 1s → σ*(NH) and N 1s → σ*(CH) from the backbone as suggested in the calculated X-ray absorption spectrum at the nitrogen K-edge of triglycine protonated at a backbone amide oxygen atom.[9]

The broad resonance centered around 406 eV for G_5 and containing N 1s → σ*(NH_3^+) transitions, is not observed in Ac-G_5. As expected, Ac-G_5 cannot adopt an NH_3^+ protonated form because of the acetylation of its N-terminus. The different protonation sites for Ac-G_5 result in a different fingerprint in its NEXAMS spectrum. Instead, we expect the proton to be located on one of the carboxyl groups of the peptide.[6] However, due to the acetylation, Ac-G_5 does not show the N 1s → σ*(NH_2) transition in the unprotonated N-terminal at 403.4 eV that we observed in backbone oxygen protonated triglycine.[9]

Finally, the resonance at 400 eV could be the signature of an N 1s → π*(C═N) excitation, as was reported for peptide-like molecules at around 399.5 eV[28] and nucleotides at around 399.7 eV.[22,41,42] Ac-G_5 sequence contains no double bond between a nitrogen and a carbon atom. A possibility for observing a π*(C═N) excitation in Ac-G_5 could be that some peptide bonds adopt an enol form, coexisting with the keto form that is considered more stable than any enol isomers.[12] Dörner *et al.* suggested that a resonance at 399.2 eV could be the signature of an enol form in the protonated pentapeptide met-enkephalin.[30]

3.2 Comparison with theoretical spectra

In this section, we compare the NEXAMS spectrum with calculated X-ray absorption spectra of possible keto and enol isomers of Ac-G_5 to shed light on the origin of the resonance at 400 eV. Ac-G_5 does not contain any basic side chain and has a capped N-terminus, which suggests that the protonation site should be on an amide oxygen.[6] From the experimental spectrum, we postulated that the existence of an enol tautomer might explain the resonance observed experimentally at 400 eV. Therefore, we built and optimized the structure of all possible enol and keto forms for each protonation site ($\mathbf{P_iE_j}$, P_i with i = Ac, 1, 2, 3, or 4 indicating the protonation site and E_j with

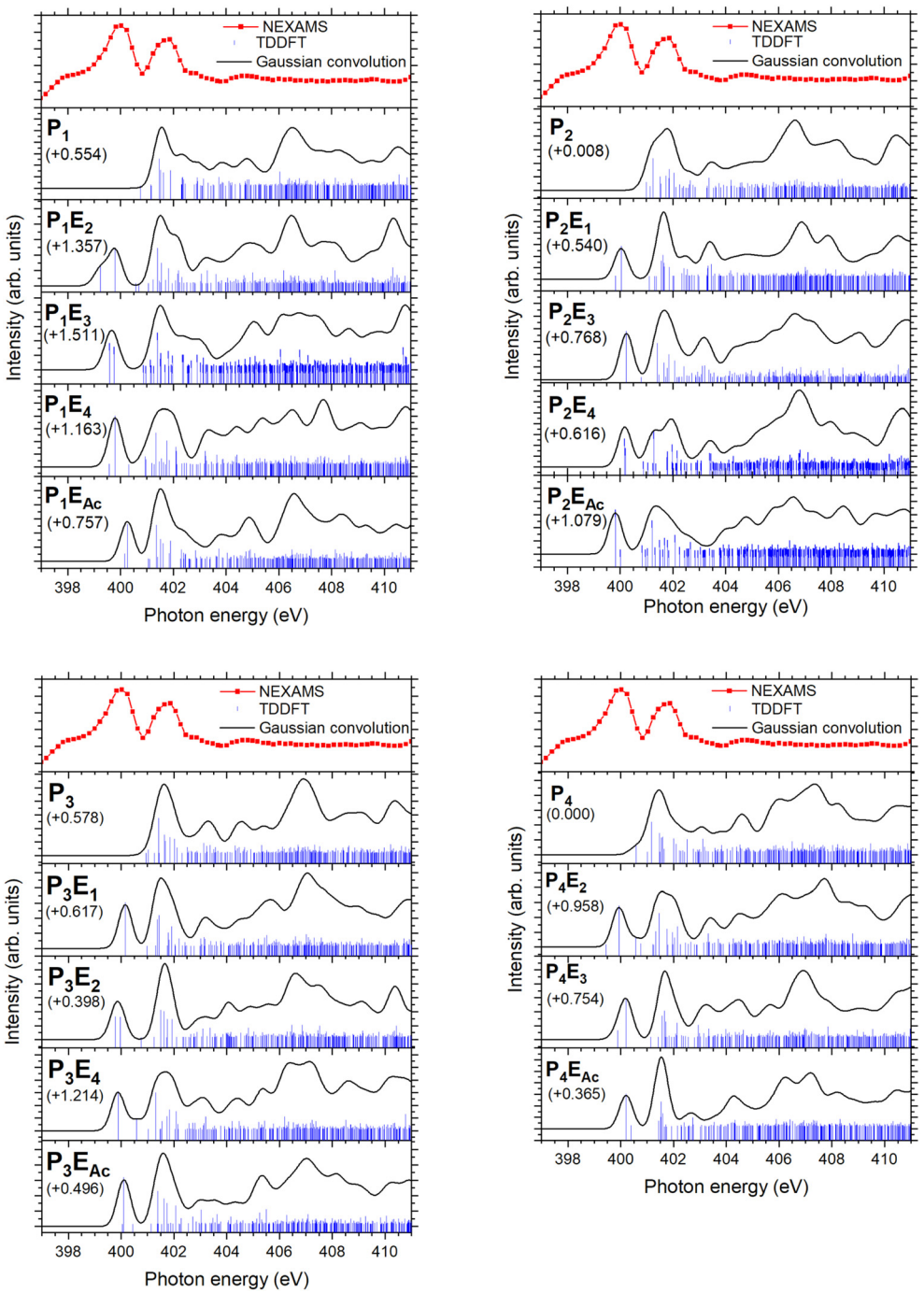

Fig. 4 Comparison of the experimental spectrum (in red) with the calculated absorption spectra of the different protomers and enol forms of Ac-G_5 at the TDDFT level of theory. The calculated spectrum of $\mathbf{P_4E_1}$ is not shown as a proton migration was observed during the calculation, and additional calculations to explore this structure were beyond the scope of this work. In parentheses, the relative electronic energy (in eV) of each structure with respect to the lowest-energy structure, $\mathbf{P_4}$, is given.

j = Ac, 1, 2, 3, or 4 indicating the position of the enol form), and calculated their X-ray absorption spectra at the N K-edge. The results of the calculations are shown in Fig. 4 and the XYZ coordinates of every analyzed structure are given in the ESI.†

While optimizing the structure protonated on the acetyl group, we observed a proton migration from the acetyl group to the second peptide bond. This could be explained by a transition state with the proton between the oxygen atom of the acetyl group and the amide oxygen of the second peptide bond. Therefore, this protomer was not further investigated. Additional calculations beyond the scope of this work are needed to explore this possible transition state.

The $\mathbf{P_4E_1}$ structure is not shown either in Fig. 4 because we observed a proton migration from the amide oxygen of the fourth peptide bond to the acetyl group. Its absorption spectrum at the N K-edge was still calculated and analyzed but did not differ from the one of the other structures. We also considered the formation of multiple enol forms, but these structures were lying at least 2.5 eV higher in energy than the single enol structures and thus were not further considered in the analysis.

All the computed absorption spectra are compared with the NEXAMS spectrum and shown in Fig. 4. For each conformer, the relative electronic energy with respect to the lowest-energy structure ($\mathbf{P_4}$) is also indicated in Fig. 4. For Ac-G_5, depending on the protonation site, the enol forms are 0.35 eV to 1 eV higher in energy than their respective keto forms, the lowest-energy one being $\mathbf{P_4E_{Ac}}$. This is consistent with the work of Wu and Lien, who performed *ab initio* calculations on the tautomerization from keto to enol of acetylated derivatives and predicted the enol form to lie $\sim$1 eV higher in energy than their respective keto form.[18] Despite some structures having relatively high electronic energy, we considered all keto forms and their relative enol forms further.

Comparing the calculated spectra of the all-keto structures ($\mathbf{P_1}$, $\mathbf{P_2}$, $\mathbf{P_3}$, and $\mathbf{P_4}$) with the experimental NEXAMS, we can see that the resonance at 400 eV is not reproduced in the calculations. The first resonance of the all-keto structures appears at 401.6 eV and has contributions from N 1s $\rightarrow$ π^*(CONH) transitions in the peptide bonds and from the protonation site according to the analysis of the TDDFT calculations. At higher energy lie the different σ^*(NH) transitions. We can already conclude that if we may have keto forms of Ac-G_5 contributing to the experimental spectrum, it is not the main isomer present under our experimental conditions.

In Fig. 4 are also shown the calculated spectra for all the structures having an enol form, for the different protonation sites of Ac-G_5. Each of the calculated enol forms shows the resonance at 400 eV and the resonance at 401.6 eV, in good agreement with the experimental spectrum. The second resonance at 401.6 eV is, for all enol forms, due to N 1s $\rightarrow$ π^*(CONH) excitation from the peptide bond or the protonation site of the peptide. For some enol forms ($\mathbf{P_1E_2}$, $\mathbf{P_2E_1}$, $\mathbf{P_2E_3}$, $\mathbf{P_2E_4}$, $\mathbf{P_3E_1}$, $\mathbf{P_3E_4}$, and $\mathbf{P_4E_2}$), the calculated spectra show a resonance around 403 eV, that could be attributed to different σ^*(NH) transitions over the backbone and the acetyl group, but no N_i 1s $\rightarrow$ π^*(CON$_j$H) type transitions.

By analyzing the various electronic transitions responsible for the band at 400 eV across all enol forms, we concluded that it primarily arises from N 1s $\rightarrow$ π^*(C═N) transitions within the enol peptide bond. Additionally, there is a contribution from the N 1s $\rightarrow$ π^*(CONH + H^+) transition associated with the protonation site of the peptide bond. However, for the structure $\mathbf{P_3E_2}$, the 400 eV resonance is solely attributed to N 1s $\rightarrow$ π^*(CONH) transitions, along with N 1s $\rightarrow$ π^*(CONH + H^+) contributions from the protonation site. This allows us to attribute unambiguously the first resonance of the experimental spectrum at 400 eV to the signature of the enol form in Ac-G_5.

Conclusions

In conclusion, we explored protonated acetyl-pentaglycine by X-ray absorption mass spectrometry at the N K-edge. By comparing it with the NEXAMS spectrum of protonated pentaglycine from our previous study,[9] we observed that the Ac-G_5 spectrum does not exhibit the resonance that can be attributed to a protonated N-terminus at 406 eV but possesses a resonance at 400 eV that was not observed for G_5. Our work allowed us to unambiguously assign this resonance to the enol form of a peptide bond in Ac-G_5. The attribution of this resonance to an N 1s $\rightarrow$ π^*(C═N) transition is in agreement with previous work for peptide-like molecules and nucleotides.[28,41,42] The presence of the enol form for acetyl-pentaglycine under our experimental conditions could be further confirmed with the support of TDDFT calculations. For all possible protonation sites, we could conclude that the calculated absorption spectra of their all-keto forms did not fit the experimental spectrum; the all-keto forms could not explain the presence of the resonance at 400 eV. However, the computed enol forms for every protonation site reproduced the resonance at 400 eV, and we could assign this resonance to N 1s $\rightarrow$ π^*(C═N) transitions from the enol forms.

From our computational and experimental results, we could not locate the exact position of the enol form in the studied protonated peptide; further exploration of the possible structures and transition states would allow us to gain more insight into the enol form formation in Ac-G_5. As already suggested,[10,11] enol formation can be assisted by the surrounding solvent or water molecules in the liquid phase, thus probing the influence of a few water molecules on the structure of Ac-G_5 could shed light on the position of the enol forms. Our present work does not answer the question of the origin of the keto–enol tautomerism in Ac-G_5. Noteworthy, the backbone protonation alone cannot explain the enolization as, for example, the X-ray absorption spectrum at the nitrogen K-edge of backbone protonated triglycine did not show such resonance at 400 eV.[9] Finally, further work at X-ray free-electron laser facilities would allow to study the dynamics of the UV-induced keto–enol tautomerism in UV pump-soft X-ray probe experiments.

Author contributions

L. S. and S. B. did the conceptualization and supervision. J. L. did the formal analysis and the theoretical calculations. J. L.,

K. S., C. O.-M., L. S., I. U., F. T., and S. B. performed the experiment at the P04 beamline of PETRA III. All authors participated in reviewing and editing the original draft written by J. L.

Data availability

The data supporting the NEXAMS experiment and the calculations have been included in the manuscript and ESI.† The individual mass spectra are available upon request from the corresponding author.

Conflicts of interest

There are no conflicts to declare.

Acknowledgements

This research was supported by the Centre for Molecular Water Science (CMWS) in an Early Science Project. J. L. acknowledges the Région Normandie (France) for funding within the NANO-HYDRAD project. F. T. acknowledges funding by the Deutsche Forschungsgemeinschaft (DFG, German Research Foundation) – Project 509471550, Emmy Noether Programme. L. S. and S. B. acknowledge funding by the Helmholtz Initiative and Networking Fund. This work is supported by the Cluster of Excellence CUI: Advanced Imaging of Matter of the Deutsche Forschungsgemeinschaft (DFG) – EXC 2056 – project ID 390715994 and Grant No. HIDSS-0002 DASHH (Data Science in Hamburg-HELMHOLTZ Graduate School for the Structure of Matter). We acknowledge DESY (Hamburg, Germany), a member of the Helmholtz Association HGF, for the provision of experimental facilities. Parts of this research were carried out at PETRA III, and we would like to thank Moritz Hoesch, Kai Bagschik, Jörn Seltmann, and Frank Scholz for their assistance in using the beamline P04. We thank Amir Kotobi for his input during the experimental campaign. Beamtime was allocated for proposal I-20191057. This research was supported in part through the Maxwell computational resources operated at Deutsches Elektronen-Synchrotron DESY, Hamburg, Germany.

Notes and references

1 K. B. Shelimov and M. F. Jarrold, *J. Am. Chem. Soc.*, 1996, **118**, 10313–10314.
2 Z. Wu and C. Fenselau, *Rapid Commun. Mass Spectrom.*, 1992, **6**, 403–405.
3 K. Zhang, D. M. Zimmerman, A. Chung-Phillips and C. J. Cassady, *J. Am. Chem. Soc.*, 1993, **115**, 10812–10822.
4 Z. Wu, C. Fenselau and R. Graham Cooks, *Rapid Commun. Mass Spectrom.*, 1994, **8**, 777–780.
5 C. Bleiholder, S. Suhai and B. Paizs, *J. Am. Soc. Mass Spectrom.*, 2006, **17**, 1275–1281.
6 H. Nair and V. H. Wysocki, *Int. J. Mass Spectrom. Ion Processes*, 1998, **174**, 95–100.
7 C. F. Rodriquez, A. Cunje, T. Shoeib, I. K. Chu, A. C. Hopkinson and K. W. M. Siu, *J. Am. Chem. Soc.*, 2001, **123**, 3006–3012.
8 H. Li, J. Jiang and Y. Luo, *Phys. Chem. Chem. Phys.*, 2017, **19**, 15030–15038.
9 J. Leroux, A. Kotobi, K. Hirsch, T. Lau, C. Ortiz-Mahecha, D. Maksimov, R. Meißner, B. Oostenrijk, M. Rossi, K. Schubert, M. Timm, F. Trinter, I. Unger, V. Zamudio-Bayer, L. Schwob and S. Bari, *Phys. Chem. Chem. Phys.*, 2023, **25**, 25603–25618.
10 Y. Takano and H. Nakamura, *Chem. Phys. Lett.*, 2006, **430**, 149–155.
11 C. F. Rodriquez, A. Cunje, T. Shoeib, I. K. Chu, A. C. Hopkinson and K. W. M. Siu, *J. Phys. Chem. A*, 2000, **104**, 5023–5028.
12 K. Kamiya, M. Boero, K. Shiraishi and A. Oshiyama, *J. Phys. Chem. B*, 2006, **110**, 4443–4450.
13 C. L. Perrin, C. P. Lollo and E. R. Johnston, *J. Am. Chem. Soc.*, 1984, **106**, 2749–2753.
14 C. L. Perrin, *Acc. Chem. Res.*, 1989, **22**, 268–275.
15 Q.-G. Li, Y. Xue and G.-S. Yan, *J. Mol. Struct. THEOCHEM*, 2008, **868**, 55–64.
16 H. Watarai and N. Suzuki, *J. Inorg. Nucl. Chem.*, 1974, **36**, 1815–1820.
17 G. W. Mines and H. W. Thompson, *Proc. R. Soc. London, Ser. A*, 1975, **342**, 327–339.
18 C.-C. Wu and M.-H. Lien, *J. Phys. Chem.*, 1996, **100**, 594–600.
19 G. Alagona, C. Ghio and P. I. Nagy, *Phys. Chem. Chem. Phys.*, 2010, **12**, 10173–10188.
20 E. Ferrari, M. Saladini, F. Pignedoli, F. Spagnolo and R. Benassi, *New J. Chem.*, 2011, **35**, 2840–2847.
21 S. Attia, M.-C. Schmidt, C. Schröder, P. Pessier and S. Schauermann, *Angew. Chem., Int. Ed.*, 2018, **57**, 16659–16664.
22 G. Mattioli, R. Schürmann, C. Nicolafrancesco, A. Giuliani and A. R. Milosavljević, *J. Phys. Chem. Lett.*, 2023, **14**, 10173–10180.
23 E. Mateo-Marti and C. M. Pradier, *Spectrochim. Acta, Part A*, 2013, **109**, 247–252.
24 G. Cooper, M. Gordon, D. Tulumello, C. Turci, K. Kaznatcheev and A. P. Hitchcock, *J. Electron Spectrosc. Relat. Phenom.*, 2004, **137–140**, 795–799.
25 Y. Zubavichus, A. Shaporenko, M. Grunze and M. Zharnikov, *J. Phys. Chem. A*, 2005, **109**, 6998–7000.
26 E. Otero and S. G. Urquhart, *J. Phys. Chem. A*, 2006, **110**, 12121–12128.
27 Y. Zubavichus, A. Shaporenko, M. Grunze and M. Zharnikov, *J. Phys. Chem. B*, 2007, **111**, 9803–9807.
28 Y.-J. Chiang, W.-C. Huang, C.-K. Ni, C.-L. Liu, C.-C. Tsai and W.-P. Hu, *AIP Adv.*, 2019, **9**, 085203.
29 L. Schwob, S. Dörner, K. Atak, K. Schubert, M. Timm, C. Bülow, V. Zamudio-Bayer, B. von Issendorff, J. T. Lau, S. Techert and S. Bari, *J. Phys. Chem. Lett.*, 2020, **11**, 1215–1221.
30 S. Dörner, L. Schwob, K. Atak, K. Schubert, R. Boll, T. Schlathölter, M. Timm, C. Bülow, V. Zamudio-Bayer, B. von Issendorff, J. T. Lau, S. Techert and S. Bari, *J. Am. Soc. Mass Spectrom.*, 2021, **32**, 670–684.

31 X. Wang, S. Rathnachalam, K. Bijlsma, W. Li, R. Hoekstra, M. Kubin, M. Timm, B. von Issendorff, V. Zamudio-Bayer, J. T. Lau, S. Faraji and T. Schlathölter, *Phys. Chem. Chem. Phys.*, 2021, **23**, 11900–11906.
32 J. Leroux, J.-Y. Chesnel, C. Ortiz-Mahecha, A. Nair, B. Oostenrijk, L. Pille, F. Trinter, L. Schwob and S. Bari, *Chem. – Eur. J.*, 2025, **31**, 202403665.
33 J. Viefhaus, F. Scholz, S. Deinert, L. Glaser, M. Ilchen, J. Seltmann, P. Walter and F. Siewert, *Nucl. Instrum. Methods Phys. Res., Sect. A*, 2013, **710**, 151–154.
34 M. F. Peintinger, D. Vilela Oliveira and T. Bredow, *J. Comput. Chem.*, 2013, **34**, 451–459.
35 A. D. Becke, *Phys. Rev. A*, 1988, **4**, 276–282.
36 F. Neese, F. Wennmohs, U. Becker and C. Riplinger, *J. Chem. Phys.*, 2020, **152**, 224108.
37 E. van Lenthe, J. G. Snijders and E. J. Baerends, *J. Chem. Phys.*, 1996, **105**, 6505–6516.
38 P. Thompson, D. E. Cox and J. B. Hastings, *J. Appl. Crystallogr.*, 1987, **20**, 79–83.
39 M. W. Buckley and N. A. Besley, *Chem. Phys. Lett.*, 2011, **501**, 540–546.
40 M. L. Gordon, G. Cooper, C. Morin, T. Araki, C. C. Turci, K. Kaznatcheev and A. P. Hitchcock, *J. Phys. Chem. A*, 2003, **107**, 6144–6159.
41 H. Shimada, T. Fukao, H. Minami, M. Ukai, K. Fujii, A. Yokoya, Y. Fukuda and Y. Saitoh, *J. Chem. Phys.*, 2014, **141**, 055102.
42 H. Shimada, T. Fukao, H. Minami, M. Ukai, K. Fujii, A. Yokoya, Y. Fukuda and Y. Saitoh, *Chem. Phys. Lett.*, 2014, **591**, 137–141.

